
HopCast: Calibration of Autoregressive Dynamics Models

Muhammad Bilal Shahid¹ Cody Fleming¹

Abstract

Deep learning models are often trained to approximate dynamical systems that can be modeled using differential equations. These models are optimized to predict one step ahead and produce calibrated predictions if the predictive model can quantify uncertainty, such as deep ensembles. At inference time, multi-step predictions are generated via autoregression, which needs a sound uncertainty propagation method (e.g., Trajectory Sampling) to produce calibrated multi-step predictions. This paper introduces an approach named HOPCAST that uses the Modern Hopfield Network (MHN) to learn the residuals of a deterministic model that approximates the dynamical system. The MHN predicts the density of residuals based on a context vector at any timestep during autoregression. This approach produces calibrated multi-step predictions without uncertainty propagation and turns a deterministic model into a calibrated probabilistic model. This work is also the first to benchmark existing uncertainty propagation methods based on calibration errors with deep ensembles for multi-step predictions.

1. Introduction

Deep learning models are becoming increasingly complex, with an explosion in the number of trainable parameters. This can result in overparameterization, in which there are more parameters than necessary to fit the training data, and can result in overfitting on a *limited* amount of data (Sagawa et al., 2020). An overfitted model can give us near-perfect training performance while making wrong predictions on the test data with high confidence (Guo et al., 2017). These overconfident predictions can be disastrous when such models are deployed as a building block in a decision-making framework for a safety-critical system,

¹ Department of Mechanical Engineering, Iowa State University, Ames, IA 50011, USA . Correspondence to: Muhammad Bilal Shahid <belal@iastate.edu>, Cody Fleming <flemingc@iastate.edu>.

Preliminary work. Under review by the International Conference on Machine Learning (ICML). Do not distribute.

such as medical diagnosis (Caruana et al., 2015). Thus, accurately estimating uncertainty in the predictive distribution is of prime importance. In this paper, we investigate uncertainty and calibration in autoregressive settings, in particular dynamics models that are typically formulated in terms of differential equations.

Calibrating the confidence of a model is tantamount to accurate estimation of the uncertainty associated with the underlying predictive variable (Gupta et al., 2006). An uncertainty-aware model is a well-calibrated model (Kumar et al., 2019). A model is *calibrated* when the expected fractions for a predictive variable match its observed fractions. For example, a 90% prediction interval should contain the observed outcome 90% of the time. It requires capturing both aleatoric and epistemic uncertainty (Hüllermeier & Waegeman, 2021). Aleatoric uncertainty is an irreducible type of uncertainty that arises due to the inherent randomness in the underlying process. In contrast, the epistemic is a reducible type of uncertainty due to lack of data. The total uncertainty is composed of an accurate estimation of both types of uncertainties (Depeweg et al., 2017).

Several methods have been devised to quantify total uncertainty, such as Bayesian methods and ensemble methods, to name a few (Abdar et al., 2021). There are three broad classes of models used in Bayesian and ensemble methods. Deterministic models have uncertainty in neither their parameters nor predictions, e.g. a classic feedforward neural network. Second, a probabilistic model has uncertainty in its predictions but not in its parameters, e.g., a neural network that predicts μ and σ , the parameters of a Gaussian. Finally, a Bayesian model has uncertainty both in its parameters and predictions.

In *Bayesian* models, a distribution over the parameters of the underlying model is learned, called posterior distribution. At inference time, multiple samples of parameters can be taken from the posterior distribution using an accurate sampling method, such as Hamiltonian Monte Carlo (HMC) (Betancourt, 2017). These samples serve as multiple predictive models and give us the desired diversity in the predictive variable of interest. A notable method from this domain is Bayes by Backprop (Blundell et al., 2015), which learns an approximate posterior distribution over the weights of a feedforward model via Variational Inference (VI) by optimizing the evidence lower bound (ELBO)

(Kingma et al., 2015).

In classical *ensemble* methods, an ensemble of models (e.g. decision trees) is trained with variations in the data for each model in the ensemble to train robust predictors (Davison & Hinkley, 1997). Deep ensembles, however, are constructed using modern deep learning models (e.g., feedforward) with random initializations in the parameter space. These over-parametrized models, when initialized randomly, converge to different local minima, giving us the desired diversity in the predictive variable (Fort et al., 2019) even though each model was trained on the same data. These models were first presented by Lakshminarayanan et al. (Lakshminarayanan et al., 2017) in the context of predictive uncertainty estimation. A notable extension of that is Neural Ensemble Search (Zaidi et al., 2021), which uses different architectures for models in an ensemble and improves upon deep ensembles.

The different uncertainty quantification methods discussed so far produce calibrated predictions with varying amounts of calibration errors. Most of these works focus on classification datasets, such as CIFAR-10, etc. Some works have results on regression problems from the UCI datasets. Sometimes, feedforward models are trained to predict system state one step ahead given the current state under Markov assumption to approximate a *dynamical system* that can be modeled using a system of ordinary differential equations (ODEs), e.g. the Lorenz System. Such a model can then predict system state multiple steps ahead at the inference time via autoregression. *Is it possible for a calibrated one-step predictive model that approximates a dynamical system to generate calibrated multi-step predictions via autoregression?* We shall answer this question using existing approaches and propose a new approach that performs competitively well.

Existing approaches to generate calibrated multi-step predictions for dynamical systems with one-step predictive models need a sound propagation method. If the predictive model is deterministic, there is no need for specialized propagation methods. On the other hand, a probabilistic model needs specialized propagation methods, such as Trajectory Sampling, Moment Matching, and Expectation. The probabilistic models with these propagation methods have been used before in Model-Based Reinforcement Learning (Chua et al., 2018). However, their calibration performance is missing from the literature to the best of our knowledge. We study these approaches from the perspective of calibration and use them as baselines.

The proposed approach to generate calibrated multi-step predictions for dynamical systems with one-step predictive models needs a base model and a residual learning model. A residual is the difference between the base model’s prediction and ground truth. We select a deterministic feedfor-

ward neural network as our base model and a Modern Hopfield Network (MHN) (Ramsauer et al., 2020) as a model that learns the residuals of the base model when used as a multi-step predictor. Precisely, the base model predicts the next state given the current state, and MHN predicts a multinomial distribution over residuals for the next state given a context vector. The context vector is made up of the current state of the dynamical system and auxiliary features. The samples from that distribution can be added to the base model’s prediction at *any timestep*. As MHN learns the residuals of the base model for multi-step predictions, it is aware of the uncertainty of the base model at any timestep. Hence, there is no need for specialized uncertainty propagation methods with the proposed approach.

Summary of Contributions The objective of this study is two-fold. An MHN-based residual learning approach, called HOPCAST, is introduced to calibrate *any* underlying one-step *deterministic* model that approximates a dynamical system for multi-step predictions. This approach is agnostic to the underlying model. We use the deterministic feedforward neural network, but it should work with other regression (e.g., decision trees) and physics-based (e.g., Lorenz95) models as well. In either case, we need a model that predicts the point estimates of the states of the system and reference observations to calculate the residuals for MHN. A secondary contribution is the study of existing one-step predictive feedforward models based on their calibration errors for multi-step predictions in the context of dynamical systems using several propagation methods, which is the first of its kind.

2. Preliminaries

2.1. Modern Hopfield Network

MHN extends classical Hopfield networks to continuous-valued patterns. A classical Hopfield network can only differentiate between binary patterns, whereas an MHN can differentiate between continuous ones. Ramsauer et al. (Ramsauer et al., 2020) proposed a new energy function for MHN:

$$E = -\text{lse}(\beta, \mathbf{X}^T \boldsymbol{\xi}) + \frac{1}{2} \boldsymbol{\xi}^T \boldsymbol{\xi} + \beta^{-1} \log N + \frac{1}{2} M^2, \quad (1)$$

where $\text{lse}(\cdot)$ denotes the LogSumExp. The matrix \mathbf{X} is constructed from N continuous stored patterns $(\mathbf{x}_1, \dots, \mathbf{x}_N)$ and M denotes the largest norm of all stored patterns. The letter $\boldsymbol{\xi}$ denotes the state pattern, which is to be associated with the stored patterns \mathbf{X} . Interestingly, the energy function can be minimized using the attention mechanism proposed by Vaswani et al. (Vaswani, 2017) as an update rule. The update rule can be derived from the energy function via Concave-Convex-Procedure. For derivation, see Ramsauer (Ramsauer et al., 2020). The update

rule can be written as:

$$\xi^{\text{new}} = \mathbf{X} \text{softmax}(\beta \mathbf{X}^T \xi) \quad (2)$$

The attention mechanism, as an update rule, plays a central role in MHN and is shown in Eq. 2. Here, the letter ξ denotes a single state pattern. For S state patterns $(\xi_1, \dots, \xi_S)^T$ denoted by Ξ , the Eq. 2 can be written as:

$$\Xi^{\text{new}} = \mathbf{X} \text{softmax}(\beta \mathbf{X}^T \Xi) \quad (3)$$

The value patterns in Eq. 2 and 3 are denoted by \mathbf{X} , which means they are the same as the state patterns \mathbf{X}^T . Depending on the problem, they could be the same or different. We have used terminology from the MHN paper to explain the update rule. Another way to look at the same update rule is from the point of view of the attention mechanism. The attention mechanism, as introduced by Vaswani et al. (Vaswani, 2017) can be defined as:

$$\hat{\mathbf{V}} = \mathbf{V} \text{softmax}\left(\frac{\mathbf{Q}\mathbf{K}}{\sqrt{d}}\right) \quad (4)$$

Eq. 4 can be compared with Eq. 3. \mathbf{K} and \mathbf{Q} , called keys and queries, respectively, correspond to the stored patterns \mathbf{X}^T and state patterns Ξ in Eq. 3. In the attention mechanism, the goal is to find the similarities of query patterns with key patterns. The similarities assigned to different keys are then multiplied with their corresponding values \mathbf{V} to produce the final output $\hat{\mathbf{V}}$. Here, we have used different letters for keys and values to be consistent with the attention mechanism equation. An intuitive understanding of keys, queries, and values, with reference to the present problem, will be given soon.

2.2. Problem Description

The objective in this paper is to calibrate a one-step predictive model for multi-step predictions. To train a one-step predictive model, the dataset is generated through a system of differential equations. One common example of a system of differential equations is the Lotka-Volterra (LV) system, which can be written as follows:

$$\frac{dx}{dt} = \alpha x - \beta xy \quad (5)$$

$$\frac{dy}{dt} = \delta xy - \gamma y \quad (6)$$

The *state* of the LV system is defined as (x, y) . An initial condition in the form of the current system state (x_0, y_0) is provided to the solver to predict t timesteps into the future. To get t timestep predictions from this system of differential equations, it must be integrated through a numerical solver. The `solve_ivp` method from `scipy` was used for integration. The following parameters were used for the system: $\alpha = 1.1, \beta = 0.4, \gamma = 0.4$, and $\delta = 0.1$. The

t for the LV system was selected as 30 with a $\Delta t = 0.1$; that is, the solver will predict 300 timesteps into the future, given the current system state. To generate a dataset with varying initial conditions, 500 initial conditions were picked randomly from the following ranges of the state variables: $x = (5, 20)$ and $y = (5, 10)$. The trajectories¹ from the system have temporal dependencies, but we would mix them together before training since we train the feedforward model like a one-step predictive model. However, a set of trajectories was kept (with temporal dependencies) since we need that to prepare a dataset for MHN training, as we shall see later. The dataset generated through differential equations was named as *Integrated*.

A feedforward model with 2 layers and 400 neurons in each layer was used to train a one-step predictive model for the LV system. A split of 80/20 was used. The feedforward model was trained to output $(\Delta x_{t+1}, \Delta y_{t+1})$ given input (x_t, y_t) , that is, the model will predict the difference between the next and previous state given the previous state of the system. The input can be added to the output to get the next state of the system, which then goes as input to the feedforward model at the next time step. Once the model is trained, it will be used in place of differential equations to generate a new data set called *Autoregressive*. The same random initial conditions will be used for the trained feedforward model, and the model will predict 300 timesteps into the future via autoregression. One could also choose to predict derivatives. In that case, the input and output of the feedforward model for the LV system is $(x_t, y_t, \dot{x}_t, \dot{y}_t)$ and $(\Delta x_{t+1}, \Delta y_{t+1}, \Delta \dot{x}_{t+1}, \Delta \dot{y}_{t+1})$, respectively. The following analysis presents results for several benchmark dynamical systems. We predict the state of the system along with derivatives for LV and Lorenz and just the state of the system for FitzHugh-Nagumo (FHN), Lorenz95, and Glycolytic Oscillator. The other systems of differential equations and their parameters are described in Appendix D. These kinds of approximations of the dynamical system are common in model-based reinforcement learning literature (Deisenroth & Rasmussen, 2011; Lu et al., 2021), with the only difference being the absence of control inputs in our problem.

3. Proposed Methodology

Residual Learning We propose to learn the residuals of the underlying deterministic one-step predictive model to

¹We will use the term trajectory for the sequence that has temporal dependencies within its elements and keep the sequence term reserved for the attention mechanism dataset. As we shall see later, the attention mechanism needs sequences to train, and the elements of a sequence do have temporal dependencies by definition. In the present work, however, the elements of a sequence in the attention mechanism have no temporal dependencies. Hence, different terms like trajectory and sequence are used.

calibrate it for multi-step predictions. This can be formulated as a pattern retrieval problem via MHN. MHN takes as input a *context pattern*, which is the current state of the system at *timestep* t augmented with auxiliary features and predicts a categorical distribution of errors (*Inference* block in Figure 1 in Appendix A). The samples are taken from that distribution to generate a probabilistic error estimate at any timestep during autoregression. These error samples can be added *directly* to the deterministic model’s prediction to get its calibrated probabilistic estimate. Note that the deterministic model is predicting a point estimate, but the error estimate from MHN is probabilistic in the form of samples from a categorical distribution which eventually turns the deterministic model into a calibrated probabilistic model. At the next time step, the deterministic model takes its *own* predicted point estimate from the previous step as input and predicts the next step, gets an error estimate from MHN, and so on.

An illustration explaining the training and inference in MHN is shown in Figure 1. Let us discuss the *Training* block first. To train the model, we need to prepare the data best suited to learning from the attention mechanism. Even though the attention mechanism processes data in sequences, it does not know the temporal dependency between patterns in a sequence² unless we explicitly do it. One way to do that is positional encoding, which adds a unique encoding to each pattern in a sequence. This encoding helps the attention mechanism learn the order of a pattern in a sequence. Sinusoidal positional encoding (Vaswani, 2017) has seen success in a variety of sequence-to-sequence tasks, although a good positional encoding is problem-dependent. Here, MHN is trained like a pattern retrieval algorithm instead of sequence-to-sequence modeling. This requires two changes. First, we used explicit timestep IDs (i.e., $t = 0, 1, 2, \dots$, etc.) as positional encoding. Second, the patterns in the sequence, after adding positional encoding, were randomly mixed. These two changes resulted in better results than sinusoidal positional encoding and maintaining the temporal order of patterns in sequences.

Since we are training a pattern retrieval algorithm, it makes sense to ask, “What constitutes a pattern?” One might say that the patterns that make *Integrated* and *Autoregressive* trajectories, which we call “raw” patterns, could be used as *key* and *query* patterns, respectively. For example, the state of the LV system is defined as (x, y) , which constitutes a raw pattern. Please note that key patterns are constructed from *Integrated* trajectories and query patterns from *Autoregressive*. It turns out that raw patterns do not

²We are using the term pattern instead of elements for the vectors that make up a sequence to be consistent with the terminology in MHN. Alternatively, these patterns could be called elements of a sequence.

give good performance. To make a pattern useful for the problem of autoregressive dynamics models, a positional encoding with initial condition and timestep ID must be included in the pattern. After these changes, an example pattern is $(x_0^3, y_0^3, x_4^3, y_4^3, t_4)$, where the superscript shows the trajectory ID and the subscript shows the timestep ID. The previous pattern corresponds to the 4th timestep of the 3rd trajectory with the first two entries as initial conditions. This is called *context pattern*. The entries of a context pattern from the *Autoregressive* trajectories are denoted with an overhead bar, e.g. $(\bar{x}_0^3, \bar{y}_0^3, \bar{x}_4^3, \bar{y}_4^3, t_4)$. *Many such context patterns from any timestep of any trajectory constitute a sequence in the MHN dataset*. Note that the sequence does not have context patterns from the same trajectory in a temporal order, i.e. the trajectories are “mixed”. The keys’ values are constructed from the errors; that is, the value for the key $(x_0^3, y_0^3, x_4^3, y_4^3, t_4)$ is $(e_{x_4^3}, e_{y_4^3})$ where $e_{x_4^3} = x_4^3 - \bar{x}_4^3$. We train a separate MHN for each entry in value vector; that is why the value vector in Figure 1 has errors of x only.

In Figure 1 (*Training* block), the key and query context patterns are shown for a sequence length of eight, forming a matrix which is denoted as the *association matrix*. The context patterns in the sequence belong to different timesteps of different trajectories. The key and query context patterns have one-to-one correspondence; that is, the *Autoregressive* context pattern in queries has its *Integrated* (or ground truth) context pattern in keys. For this reason, the diagonal entries have a probability of zero, as in we use a mask and do not want the attention mechanism to pay attention to the *Integrated* pattern of an *Autoregressive* pattern. Without this masking it is trivial for the attention mechanism to minimize the loss. With this masking, we attempt to entice the mechanism to pay attention to *other* patterns to learn a generalizable sense of similarity beyond the “self” instances of trajectories. The rows in the association matrix represent categorical distributions with a length of the bar corresponding to the magnitude of probability; that is, a longer bar means higher probability and vice versa. Here, a higher probability means the query is similar to that key with a high probability. These probabilities assigned to each key are then multiplied by their corresponding values (or errors) to output the predicted error. The predicted error ($\hat{e}_{x_4^3}$) should be close to the $e_{x_4^3}$ which is the error associated with the first query $(\bar{x}_0^3, \bar{y}_0^3, \bar{x}_4^3, \bar{y}_4^3, t_4)$. The MHN will learn to predict that by paying attention to the rest of the 7 keys in the sequence.

At inference time (*Inference* block in Figure 1), a *subset* of key context patterns randomly sampled from the set of key context patterns, whose size is the same as the size of the training set, is loaded into the memory of the model called *Associative Memory* in MHN terminology. A query is given to MHN, and it finds associations for the query

with keys in memory. The resulting association is in the form of categorical distribution. Each key has its value (or error) in the memory which will be sampled with the probabilities in the categorical distribution. Even though some training datasets have sizes as big as 240,000, a small subset of context patterns, that is, 5000, was loaded into the association memory. Unlike non-parametric methods like Gaussian Processes, there is no need to load entire data into the memory. We attribute this efficiency of our method to the sequences not consisting of data points in strict temporal ordering at the training time. Without exposing a query to the keys, not in strict temporal ordering at the training time, it would have been harder for a query to find an association from a randomly sampled set of key context patterns.

In Figure 1, context vectors are shown in raw form as they did not pass through any encoding network to learn a new set of embeddings. This makes the illustration easier to understand with features of physical meanings. An encoding network of one feedforward layer with 100 neurons achieves solid performance. The context vector for each system was encoded to a dimension of 4 for all benchmarks. The same network with the same output dimension was used for all systems except Lorenz95, which sees good results with only one neuron in the layer and no activation function. The number of timesteps used as positional encoding does not have to be the current timestep only, as shown in Fig. 1; it could consist of past p timesteps. We used the past 5 timesteps as a positional encoding in the context vector for every benchmark. The only hyperparameter in our approach is the sequence length, and it can be hand-tuned without Bayesian Optimization, as we shall see later. To train MHN, an 80/20 split was used where the 80% split contains the same data that was used to train the base deterministic model, likewise for the 20% split.

4. Baseline methods for comparison

Our baseline methods include ensemble methods, both deterministic and probabilistic. We discussed Bayesian methods in section 1, but these methods, when approximating posterior distribution over parameters, do not perform as well as deep ensembles. The reason is that the samples from the approximate posterior distribution over parameters are not as diverse because Variational inference does a single-basin approximation even if the underlying posterior distribution is multi-basin. An exhaustive Hamiltonian Monte Carlo (HMC) gives a relatively good approximation that falls close to deep ensembles in terms of predictive uncertainty estimation. The downside is that HMC tends to be prohibitively expensive, whereas deep ensembles are a simple and scalable method for predictive uncertainty estimation. A detailed analysis of deep ensembles and their

comparison to Bayesian methods can be found in (Wilson & Izmailov, 2020).

With the deterministic ensemble, each model in the ensemble predicts a point estimate, and the only variance is empirical from the disagreement of models’ predictions. On the other hand, a probabilistic model predicts the mean and variance for a predictive variable. Thus, there is a predicted variance and a variance from the disagreement between the model’s predictions. The total predictive variance for a probabilistic model comprises these two variances. The latter predictive variance outperformed the empirical variance in calibration for one-step predictions (Lakshminarayanan et al., 2017). We will evaluate the calibration of these models when used for multi-step predictions.

When the underlying model is probabilistic, we must consider propagating uncertainty to get calibrated multi-step predictions. As we show later, the propagation method greatly impacts the calibration error. There are three propagation methods considered below. To propagate uncertainty, we make multiple copies of the same initial condition (\mathbf{s}_0), that is, $\{\{\mathbf{s}_0^{p,m}\}_{p=1}^P\}_{m=1}^M$. Next, we distribute the same copies equally across all models in an ensemble, as shown in Figure 2 in Appendix E. The state variable $\mathbf{s}_0^{p,m}$ denotes the p^{th} copy of the initial condition belonging to model m , for instance, $\mathbf{s}_0^{p,m} = (x_0 \ y_0)$. Informally, model m can have P/M “particles”. The next state of the system at timestep $t + 1$ is $\mathbf{s}_{t+1}^{p,m} \sim \mathcal{N}([f_\theta^m(\mathbf{s}_t^{p,m})]_\mu, [f_\theta^m(\mathbf{s}_t^{p,m})]_\sigma)$, where the probabilistic model $f_\theta^m(\cdot)$ is parameterized by θ and represents m^{th} model. With this background, there are three widely used propagation methods:

- **Expectation (E):** In this approach, the expectation (or predicted mean) is propagated, and uncertainty in the predictive variable is ignored; that is, we propagate $\mathbf{s}_{t+1}^{p,m} = [f_\theta^m(\mathbf{s}_t^{p,m})]_\mu$. An illustration of this approach is shown in Fig. 2(b) for 2 models with three particles for each, in which $\mathbf{s}_0^{1,1}$ denotes the first particle belonging to model 1. The model prediction is a multivariate normal distribution (MVN) whose dimensions depend on the state of the system. The mean prediction corresponding to the input ($\mathbf{s}_0^{1,1}$) is $\mu_1^{1,1}$ which becomes the input to the model 1 at the next time step. This is repeated until the system states for all n timesteps are predicted autoregressively. Since the uncertainty in the predicted distribution is ignored, only a single particle for each model is required. This results in reduced computation. The downside is that the prediction intervals at each time step are too conservative, as they do not consider and propagate predicted uncertainty.
- **Moment Matching (MM):** While propagating the expected value is computationally cheaper, it does not

generate calibrated intervals. A straightforward way to deal with this is to propagate *multiple* particles through each model (e.g., $s_0^{1,1}$, $s_0^{2,1}$, and $s_0^{3,1}$), take *one* sample (e.g., $s_1^{1,1}$) from each predictive distribution (e.g., $\text{MVN}(\mu_1^{1,1}, \Sigma_1^{1,1})$), force a Gaussian distribution on the particles from all models $\text{MVN}(\mu_1, \Sigma_1)$, and resample the same number of particles to propagate at the next time step (shown in blue color). That is, $s_{t+1}^{p,m} \sim \mathcal{N}(\mathbb{E}_{p,m}[f_\theta^m(s_t^{p,m})], \mathbb{V}_{p,m}[f_\theta^m(s_t^{p,m})])$ for each dimension of MVN at each timestep. An illustration of that is shown in Fig. 2(c), where the stated process is repeated n times to predict system states autoregressively. This is the moment matching w.r.t particles and models. One could retain multimodality by fitting kernel density estimation (KDE) to the set of particles, but this requires more computation as optimizing kernel bandwidth is an expensive task.

- **Trajectory Sampling (TS):** The propagation of expectation and Gaussian MM do not truly represent calibrated uncertainty because they do not capture the multi-modal distribution of uncertainties at each timestep and/or do not capture non-Gaussian densities. In TS, this can be addressed by propagating *multiple* particles through each model like MM (e.g., $s_0^{1,1}$, $s_0^{2,1}$, and $s_0^{3,1}$), take one sample (e.g., $s_1^{1,1}$) from each predictive distribution (e.g., $\text{MVN}(\mu_1^{1,1}, \Sigma_1^{1,1})$), and then propagating the sampled set of particles through their respective models as such without moment matching. That is, $s_{t+1}^{p,m} \sim \mathcal{N}([f_\theta^m(s_t^{p,m})]_\mu, [f_\theta^m(s_t^{p,m})]_\sigma)$ for each dimension of MVN at each timestep. An illustration of that is shown in Fig. 2(d), where the stated process is repeated n times to predict system states autoregressive. This retains the multi-modal nature of the particles at any timestep, which is a more realistic and general assumption than moment matching.

With a deterministic model, a single particle is required ($s_0^{1,1}$), similar to the propagation of expectation. The model predicts the next state of the system ($s_1^{1,1}$), which is then passed to the model as input at the next time step. The process is repeated until all n states of the system are predicted autoregressively. An illustration is shown in Fig. 2(a). The propagation of expectation and the deterministic ensemble are nearly equivalent, except that the former gives aleatoric uncertainty in the form of variances of MVN, which adds up to total uncertainty.

5. Experimental Results

5.1. Datasets

We tested HOPCAST and baseline models on five dynamical systems. One of the dynamical models, that is, LV, was

discussed in section 2.2. Other dynamical systems include Lorenz, FitzHugh-Nagumo, Lorenz95, and Glycolytic Oscillator. All these dynamics can be described using a system of ordinary differential equations (ODEs). Each model was integrated using `solve_ivp` from `scipy` for a different number of timesteps. Different numbers of trajectories were generated. The details about that are given in Appendix C. For each model, its system of ODEs is given in the Appendix D along with their parameter values and ranges of initial conditions.

5.2. Metrics

Three metrics are used to assess the quality of the prediction intervals (PIs) generated by HOPCAST and baseline methods: Prediction interval width (PI-Width) (Ramsauer et al., 2020), Calibration error (CE) (Kuleshov et al., 2018), and Mean Squared Error (MSE), each of which should be minimized. A detailed discussion of the metrics is in Appendix F.

5.3. Comparison to Baselines

Table 1 shows the results of HOPCAST against the baseline models. As discussed in section 5.2, there are three metrics to evaluate the performance of the HOPCAST against the baselines. Two of the metrics that is, CE and PI-Width, are reported in Table 1. Models with the best performance based on the CE are in bold. To identify best performance, we pick the model with the lowest CE and highlight any CE within 5% of it. CE is the prime criterion for picking the best model, and PI-Width is the tiebreaker. That is, if there are multiple models with CEs in the 5% range of the best one, the sharpest one based on PI-Width is the winner. In that case, the PI-Width is highlighted, CE has an asterisk in its superscript, and that model is deemed the best. An example is the Lorenz system at $\sigma = 0.3$, where HOPCAST and trajectory sampling perform best based on CE, but HOPCAST wins based on sharpness. There are a total of 15 cases, that is, five dynamical models with three levels of noise. HOPCAST has the best performance in 10 out of 15 cases. The trajectory sampling and propagation of expected value perform relatively well in a few cases, with the former winning in two and the latter in three. The deterministic ensemble did not outperform in any case due to the lack of predictive variance, but it performs fairly well when the noise is low, that is, $\sigma = 0.05$. The propagation of expectation with probabilistic ensemble and deterministic ensemble only differ in terms of aleatoric uncertainty. The propagation of expectation, therefore, achieves better calibration than deterministic ensembles.

We have seen the performance of HOPCAST against the baseline models on two metrics, that is, PI-Width and CE. A third metric, discussed in section 5.2, is important be-

HopCast: Calibration of Autoregressive Dynamics Models

Model	HOPCAST		Deterministic Ensemble		Probabilistic Ensemble						
					Expectation		Moment Matching		Trajectory Sampling		
Metrics	PI-Width	CE	PI-Width	CE	PI-Width	CE	PI-Width	CE	PI-Width	CE	
Lotka Volterra	$\sigma = 0.05$	3.05 ± 0.17	$0.018 \pm 0.004^*$	2.59 ± 0.13	0.54 ± 0.26	4.01 ± 0.40	0.017 ± 0.009	0.65 ± 0.06	0.56 ± 0.12	5.43 ± 0.10	0.22 ± 0.11
	$\sigma = 0.1$	1.95 ± 0.05	0.0073 ± 0.002	0.18 ± 0.008	2.03 ± 0.25	0.83 ± 0.02	0.47 ± 0.17	0.96 ± 0.04	0.41 ± 0.14	5.87 ± 0.59	0.18 ± 0.10
	$\sigma = 0.3$	3.35 ± 0.12	0.0071 ± 0.004	0.17 ± 0.03	2.49 ± 0.09	2.13 ± 0.02	0.21 ± 0.05	2.93 ± 0.02	0.059 ± 0.02	6.19 ± 0.22	0.13 ± 0.07
Lorenz	$\sigma = 0.05$	29.19 ± 0.74	0.011 ± 0.006	28.58 ± 0.39	0.010 ± 0.005	30.37 ± 0.80	0.002 ± 0.001	4.45 ± 0.009	1.23 ± 0.07	38.79 ± 0.49	0.16 ± 0.04
	$\sigma = 0.1$	36.85 ± 0.38	0.04 ± 0.03	28.50 ± 0.82	0.19 ± 0.08	35.49 ± 1.11	0.011 ± 0.015	8.78 ± 0.01	1.21 ± 0.08	45.28 ± 0.69	0.078 ± 0.03
	$\sigma = 0.3$	40.44 ± 0.91	$0.019 \pm 0.004^*$	10.56 ± 0.41	1.39 ± 0.24	25.9 ± 1.43	0.38 ± 0.10	23.13 ± 0.06	0.58 ± 0.30	48.52 ± 0.35	0.018 ± 0.016
FHN	$\sigma = 0.05$	0.21 ± 0.005	0.014 ± 0.004	0.53 ± 0.16	0.099 ± 0.064	1.13 ± 0.061	0.044 ± 0.034	0.28 ± 0.007	0.91 ± 0.42	1.25 ± 0.007	0.054 ± 0.026
	$\sigma = 0.1$	1.03 ± 0.05	0.28 ± 0.05	0.92 ± 0.15	0.31 ± 0.22	0.76 ± 0.064	0.38 ± 0.19	0.38 ± 0.003	1.42 ± 0.086	1.35 ± 0.003	0.051 ± 0.02
	$\sigma = 0.3$	1.27 ± 0.03	0.11 ± 0.02	0.68 ± 0.04	1.003 ± 0.33	1.009 ± 0.046	0.39 ± 0.13	1.52 ± 0.010	0.108 ± 0.019	1.55 ± 0.004	0.061 ± 0.011
Lorenz95	$\sigma = 0.05$	4.41 ± 0.13	0.008 ± 0.003	2.86 ± 0.02	0.22 ± 0.02	3.25 ± 0.015	0.13 ± 0.017	1.84 ± 0.009	0.62 ± 0.04	4.90 ± 0.023	0.022 ± 0.007
	$\sigma = 0.1$	5.78 ± 0.018	0.0028 ± 0.007	3.04 ± 0.05	0.41 ± 0.02	3.29 ± 0.05	0.27 ± 0.025	3.24 ± 0.03	0.35 ± 0.06	5.44 ± 0.04	$0.004 \pm 0.003^*$
	$\sigma = 0.3$	6.03 ± 0.06	0.0033 ± 0.001	3.72 ± 0.19	0.37 ± 0.13	4.61 ± 0.04	0.13 ± 0.029	6.01 ± 0.03	0.0036 ± 0.003	6.49 ± 0.047	0.009 ± 0.006
Glycolytic Oscillator	$\sigma = 0.05$	0.20 ± 0.007	0.038 ± 0.018	0.17 ± 0.01	0.10 ± 0.07	0.24 ± 0.02	0.07 ± 0.04	0.056 ± 0.002	1.35 ± 0.32	0.36 ± 0.006	0.06 ± 0.026
	$\sigma = 0.1$	0.25 ± 0.007	0.013 ± 0.006	0.21 ± 0.002	0.19 ± 0.02	0.21 ± 0.01	0.10 ± 0.03	0.08 ± 0.004	0.99 ± 0.18	0.41 ± 0.01	0.07 ± 0.03
	$\sigma = 0.3$	0.38 ± 0.008	0.005 ± 0.003	0.25 ± 0.19	0.44 ± 0.10	0.23 ± 0.01	0.62 ± 0.28	0.21 ± 0.003	0.54 ± 0.07	0.46 ± 0.003	0.015 ± 0.01
Average CE	-	0.038	-	0.65	-	0.21	-	0.68	-	0.075	

Table 1. Prediction Interval Widths (PI-Widths) and Calibration Error (CE) metrics on different models with varying levels of noise across various models

cause the accuracy of a regression model is often equally important. To this end, we pick the expectation of the predicted densities at any timestep during autoregression and compare it with the ground truth to calculate the MSE. As shown in Table 3, the HOPCAST outperforms baseline models in 10 out of 15 cases. In 2 cases, it performs as well as baseline models. As in Table 1, we pick the best model and highlight any other from the same row within 5%. HOPCAST not only generally outperforms baseline models in terms of CE but also in terms of MSE. This illustrates the expressive power of HOPCAST’s pattern-retrieval mechanism for residual learning as an approach toward the calibration of autoregressive dynamics models.

5.4. Hyperparameter Tuning

The sequence length used to train MHN plays a crucial role in calibrating the uncertainty. Therefore, an optimal sequence length must be determined depending on the problem at hand. Table 4 shows the optimal sequence length (Seq. Len.) for each system and noise level. The optimal sequence length for each case was tuned without the use of Bayesian Optimization, though this is a hyperparameter. The reason we tuned sequence length without the use of Bayesian Optimization is its straightforward relation with confidence. As sequence length increases, the model starts

to become underconfident and vice versa, i.e. confidence is monotonic with respect to sequence length. We simply picked a long sequence length (like 900) and a short sequence length (like 50) and observe the CE. With sufficiently small CE, the sequence length does not need to be modified as it corresponds to near perfect calibration. Otherwise, the sequence length can be selected somewhere between 50 and 900. With this approach, we found a sequence length with reasonable performance in 3 to 4 trials in most cases. CE is scale invariant to the problem setting; that is, the expected and observed fractions have the same scale irrespective of the underlying problem, so the same approach can be used for any underlying system. For perfect calibration, Bayesian optimization can be used with CE as the objective and sequence length as the hyperparameter. An intuitive understanding of the sequence length with reference to a term we introduce called *Attention Span* can be found in Appendix G.

The architecture of the encoding network for MHN (1 Layer with 100 neurons) was kept the same for all experiments except Lorenz95, as discussed earlier. To construct ensembles (both deterministic and probabilistic), 2 layers with 400 neurons each were used for base models of LV and FHN, and 3 layers with 400 neurons for Lorenz, Lorenz95, and Glycolytic Oscillator. The architecture of models in an

ensemble (both deterministic and probabilistic) is kept the same for the same system, irrespective of the noise level. The number of models in an ensemble is a hyperparameter, but we have noticed that Deterministic Ensemble, Expectation, and Moment Matching remained overconfident even after we kept increasing the number of models from a population of models, though their uncertainties did increase with the increase in the number of models. After a certain number of models, which varies from one system to another, the uncertainty plateaus, and adding more models did not improve the CE. Therefore, we kept the number of models to that fixed number where performance saturates. On the other hand, the Trajectory Sampling was able to provide calibrated uncertainty with very few models in an ensemble (e.g. 3 or 4) for most cases, which shows the importance of the propagation method. Adding more models to the ensemble did not significantly impact CE for Trajectory Sampling.

6. Discussion

We have proposed a pattern-retrieval mechanism called HOPCAST to turn a one-step deterministic neural network into a calibrated probabilistic model for multi-step predictions in the context of dynamical systems. A Modern Hopfield Network is trained on the residuals of the underlying deterministic model and learns to predict the residuals associated with the predictive variable of interest. It predicts the density of residuals based on the context information at any timestep during autoregression without the propagation of uncertainty. This approach is in contrast to the probabilistic ensemble that trains multiple predictive models with a scoring rule to quantify uncertainty. The uncertainty associated with one-step predictions must be propagated through multiple steps via uncertainty propagation methods for calibrated multi-step predictions.

A similar approach to ours was used by Auer (Auer et al., 2023) to turn a deterministic model into a calibrated one-step probabilistic model for one-step forecasts. Our approach extends that work to calibrate one-step deterministic predictive models that approximate dynamical system for multi-step predictions via autoregression. We specifically introduce the concept of *Attention Span* and how tuning it can give us calibrated error density estimates for the underlying deterministic predictive model. The sequence length and its effect on predicted densities are not mentioned in the (Auer et al., 2023), which is a key hyperparameter in our work. Based on the empirical results in the paper, there are several future avenues to extend this work.

- In this paper, we tune the sequence length to get calibrated error density estimates. If there were a way to get calibrated density estimates without changing the sequence length, it would be computationally

cheaper. One way of doing this is to train the network with strictly proper scoring rules (Gneiting & Raftery, 2007).

- Explicit timestep IDs were used as positional encoding in MHN, which restricts the model’s generalizability to trajectories that are equal to or less than the length of the trajectories it was trained on. A positional encoding that is invariant to trajectory length for residual learning would be an interesting direction.
- We prepared the *context pattern* using initial conditions, current system state, and past five timesteps. An alternative approach is to use the past few systems states as a *context pattern* and use Conv1d to learn a fixed-length embedding. This approach did not generate useful results. However, an approach along the same lines could give generalizable *context patterns* to predict errors for trajectories longer than in the dataset.

7. Related Works

Calibration has been studied widely for classification models. In binary classification, Platt Scaling (Platt et al., 1999) and isotonic regression (Niculescu-Mizil & Caruana, 2005) have been used successfully for recalibration. There are extensions of such works to multi-class classification problems (Zadrozny & Elkan, 2002). Guo et al (Guo et al., 2017) studied that the modern neural network in the age of overparameterization tends to be overconfident predictors of class probabilities compared to neural networks from decades ago. The temperature scaling – a single-parameter variant of Platt Scaling – was introduced as a fix.

These papers evaluate their approaches to classification datasets such as CIFAR-10, CIFAR-100, and the like. Gneiting et al. (Gneiting & Raftery, 2007) proposed several proper scoring rules to evaluate the calibration of a probabilistic model for continuous variables. Those scoring rules have been used in the literature as loss functions, for example continuous ranked probability score (CRPS) (Gasthaus et al., 2019) and others. Calibration has also been extensively discussed in the literature on probabilistic forecasting, mainly in the context of meteorology (Gneiting & Raftery, 2005). These papers do not focus on generating calibrated forecasts. An approach called calibrated regression was proposed by Kuleshov et al. (Kuleshov et al., 2018), which used isotonic regression to calibrate Bayesian models. In contrast, our work turns a deterministic model into a calibrated probabilistic model via MHN.

Impact Statement

This paper presents work whose goal is to advance the field of Machine Learning. There are many potential societal consequences of our work, none which we feel must be specifically highlighted here.

References

- Abdar, M., Pourpanah, F., Hussain, S., Rezazadegan, D., Liu, L., Ghavamzadeh, M., Fieguth, P., Cao, X., Khosravi, A., Acharya, U. R., et al. A review of uncertainty quantification in deep learning: Techniques, applications and challenges. *Information fusion*, 76:243–297, 2021.
- Angelopoulos, A. N., Bates, S., et al. Conformal prediction: A gentle introduction. *Foundations and Trends® in Machine Learning*, 16(4):494–591, 2023.
- Auer, A., Gauch, M., Klotz, D., and Hochreiter, S. Conformal prediction for time series with modern hopfield networks. *Advances in Neural Information Processing Systems*, 36:56027–56074, 2023.
- Betancourt, M. A conceptual introduction to hamiltonian monte carlo. *arXiv preprint arXiv:1701.02434*, 2017.
- Blundell, C., Cornebise, J., Kavukcuoglu, K., and Wierstra, D. Weight uncertainty in neural network. In *International conference on machine learning*, pp. 1613–1622. PMLR, 2015.
- Brunton, S. L., Proctor, J. L., and Kutz, J. N. Discovering governing equations from data by sparse identification of nonlinear dynamical systems. *Proceedings of the national academy of sciences*, 113(15):3932–3937, 2016.
- Caruana, R., Lou, Y., Gehrke, J., Koch, P., Sturm, M., and Elhadad, N. Intelligible models for healthcare: Predicting pneumonia risk and hospital 30-day readmission. In *Proceedings of the 21th ACM SIGKDD international conference on knowledge discovery and data mining*, pp. 1721–1730, 2015.
- Chua, K., Calandra, R., McAllister, R., and Levine, S. Deep reinforcement learning in a handful of trials using probabilistic dynamics models. *Advances in neural information processing systems*, 31, 2018.
- Daniels, B. C. and Nemenman, I. Efficient inference of parsimonious phenomenological models of cellular dynamics using s-systems and alternating regression. *PLoS one*, 10(3):e0119821, 2015.
- Davison, A. C. and Hinkley, D. V. *Bootstrap methods and their application*. Number 1. Cambridge university press, 1997.
- Deisenroth, M. and Rasmussen, C. E. Pilco: A model-based and data-efficient approach to policy search. In *Proceedings of the 28th International Conference on machine learning (ICML-11)*, pp. 465–472, 2011.
- Depeweg, S., Hernández-Lobato, J. M., Doshi-Velez, F., and Udluft, S. Uncertainty decomposition in bayesian neural networks with latent variables. *arXiv preprint arXiv:1706.08495*, 2017.
- Fort, S., Hu, H., and Lakshminarayanan, B. Deep ensembles: A loss landscape perspective. *arXiv preprint arXiv:1912.02757*, 2019.
- Gasthaus, J., Benidis, K., Wang, Y., Rangapuram, S. S., Salinas, D., Flunkert, V., and Januschowski, T. Probabilistic forecasting with spline quantile function rnns. In *The 22nd international conference on artificial intelligence and statistics*, pp. 1901–1910. PMLR, 2019.
- Gneiting, T. and Raftery, A. E. Weather forecasting with ensemble methods. *Science*, 310(5746):248–249, 2005.
- Gneiting, T. and Raftery, A. E. Strictly proper scoring rules, prediction, and estimation. *Journal of the American statistical Association*, 102(477):359–378, 2007.
- Guo, C., Pleiss, G., Sun, Y., and Weinberger, K. Q. On calibration of modern neural networks. In *International conference on machine learning*, pp. 1321–1330. PMLR, 2017.
- Gupta, H. V., Beven, K. J., and Wagener, T. Model calibration and uncertainty estimation. *Encyclopedia of hydrological sciences*, 2006.
- Hüllermeier, E. and Waegeman, W. Aleatoric and epistemic uncertainty in machine learning: An introduction to concepts and methods. *Machine learning*, 110(3): 457–506, 2021.
- Izhikevich, E. M. and FitzHugh, R. FitzHugh-Nagumo model. *Scholarpedia*, 1(9):1349, 2006. doi: 10.4249/scholarpedia.1349. revision #123664.
- Kingma, D. P., Salimans, T., and Welling, M. Variational dropout and the local reparameterization trick. *Advances in neural information processing systems*, 28, 2015.
- Kuleshov, V., Fenner, N., and Ermon, S. Accurate uncertainties for deep learning using calibrated regression. In *International conference on machine learning*, pp. 2796–2804. PMLR, 2018.
- Kumar, A., Liang, P. S., and Ma, T. Verified uncertainty calibration. *Advances in Neural Information Processing Systems*, 32, 2019.

- Lakshminarayanan, B., Pritzel, A., and Blundell, C. Simple and scalable predictive uncertainty estimation using deep ensembles. *Advances in neural information processing systems*, 30, 2017.
- Lorenz, E. N. Predictability: A problem partly solved. In *Proc. Seminar on predictability*, volume 1. Reading, 1996.
- Lu, C., Ball, P. J., Parker-Holder, J., Osborne, M. A., and Roberts, S. J. Revisiting design choices in off-line model-based reinforcement learning. *arXiv preprint arXiv:2110.04135*, 2021.
- Niculescu-Mizil, A. and Caruana, R. Predicting good probabilities with supervised learning. In *Proceedings of the 22nd international conference on Machine learning*, pp. 625–632, 2005.
- Platt, J. et al. Probabilistic outputs for support vector machines and comparisons to regularized likelihood methods. *Advances in large margin classifiers*, 10(3):61–74, 1999.
- Ramsauer, H., Schäfl, B., Lehner, J., Seidl, P., Widrich, M., Adler, T., Gruber, L., Holzleitner, M., Pavlović, M., Sandve, G. K., et al. Hopfield networks is all you need. *arXiv preprint arXiv:2008.02217*, 2020.
- Sagawa, S., Raghunathan, A., Koh, P. W., and Liang, P. An investigation of why overparameterization exacerbates spurious correlations. In *International Conference on Machine Learning*, pp. 8346–8356. PMLR, 2020.
- Vaswani, A. Attention is all you need. *Advances in Neural Information Processing Systems*, 2017.
- Wangersky, P. J. Lotka-volterra population models. *Annual Review of Ecology and Systematics*, 9:189–218, 1978.
- Wilson, A. G. and Izmailov, P. Bayesian deep learning and a probabilistic perspective of generalization. *Advances in neural information processing systems*, 33: 4697–4708, 2020.
- Zadrozny, B. and Elkan, C. Transforming classifier scores into accurate multiclass probability estimates. In *Proceedings of the eighth ACM SIGKDD international conference on Knowledge discovery and data mining*, pp. 694–699, 2002.
- Zaidi, S., Zela, A., Elsken, T., Holmes, C. C., Hutter, F., and Teh, Y. Neural ensemble search for uncertainty estimation and dataset shift. *Advances in Neural Information Processing Systems*, 34:7898–7911, 2021.

A. MHN Association Mechanism

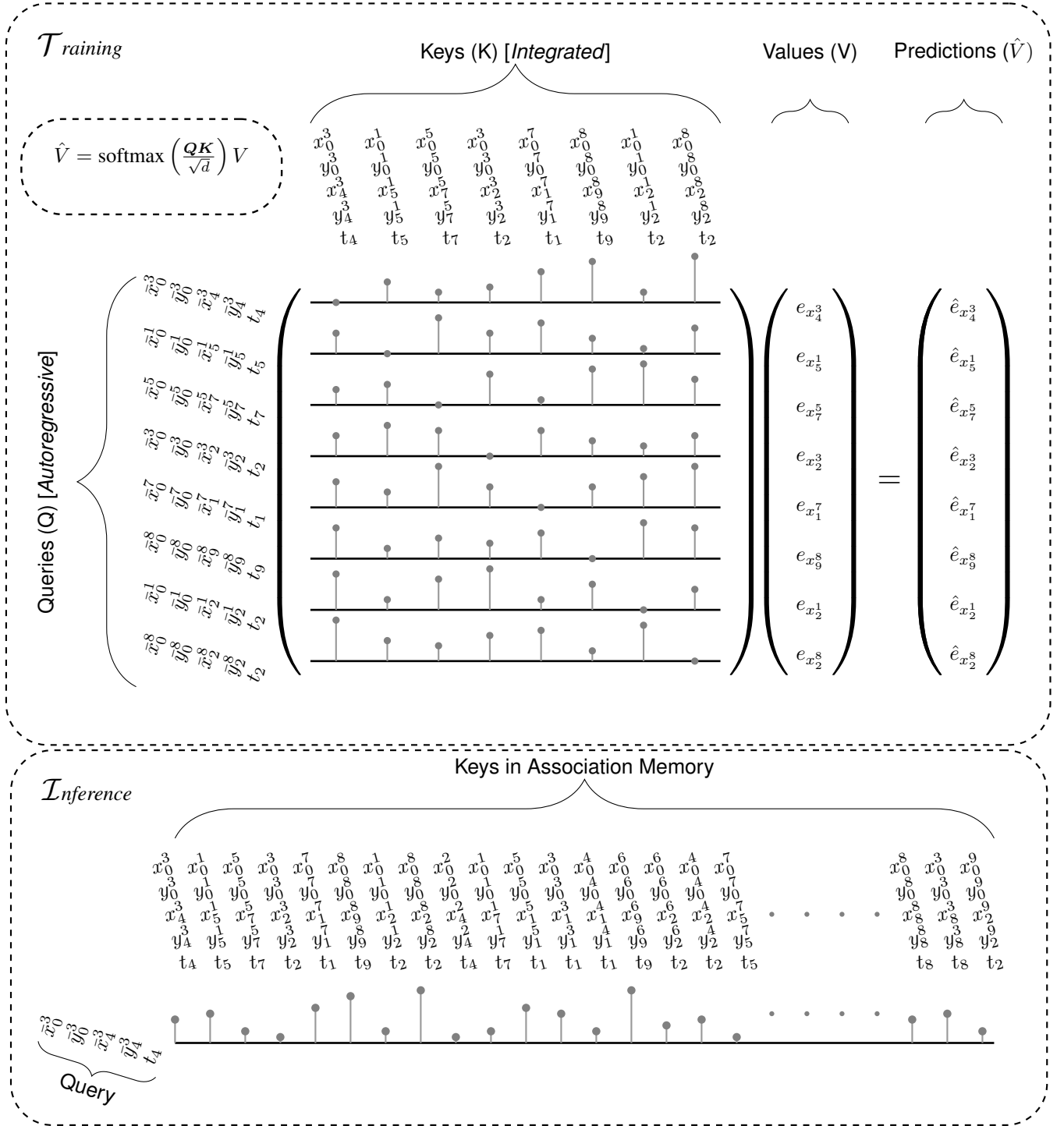


Figure 1. **MHN Association Mechanism:** In the training mode, the MHN learns to associate query patterns with key patterns via the attention mechanism. In the testing mode, a query is exposed to a few keys in the memory, and the model outputs similarities in the form of categorical distribution. A few samples are taken from this distribution to form error density.

B. PyTorch pseudocode for HOPCAST

```

# B: Batch size
# seq: Sequence length
# out: State dimension
# X.int: Integrated States
# X.auto: Autoregressive States
# errors: |X.int - X.auto|
class Train(nn.Module):
    def __init__(self, encoder, MHN, X.int, X.auto, errors):
        self.encoder = encoder # MLP
        self.K = X.int # Keys [B, seq, out]
        self.Q = X.auto # Queries [B, seq, out]
        self.V = error # Values [B, seq, 1]
        self.loss = nn.MSELoss()
        # Add Positional Encoding
        # Add Initial Conditions
    def forward(self):
        for epoch in range(40):
            # Single batch, minibatch in practice
            K.enc = self.encoder(K) # [B, seq, 4]
            Q.enc = self.encoder(Q) # [B, seq, 4]
            assoc.mat = torch.bmm(Q.enc, K.enc) # [seq, seq]
            # Use Dropout to promote sparsity
            assoc.mat = nn.functional.dropout(assoc.mat)
            ê = torch.bmm(assoc.mat, self.V) # [B, seq, 1]
            loss = self.loss(ê, self.V)
            loss.backward()

class Inference(nn.Module):
    def __init__(self, encoder, MHN, X.int, X.q, errors):
        # First Ten sequence with mixed data
        # Any sequence in practice
        self.assoc.K = X.int[:10].reshape(-1, out)
        self.assoc.V = errors[:10]
        self.X.q = X.q # Test Query
        # Add Positional Encoding
        # Add Initial Conditions
    def forward(self):
        assoc.K.enc = self.encoder(self.assoc.K)
        X.q.enc = self.encoder(self.X.q)
        assoc.mat = torch.bmm(X.q.enc, assoc.K.enc)
        # Sample from categorical distribution
        err.idx = torch.multinomial(assoc.mat)
        err.samp = self.assoc.V(err.idx)
        # Sampled errors form a distribution
        # Add directly to Predicted Next State
        # from Underlying Predictive Model

```

C. Data Generation

To generate a dataset from differential equations in Appendix D, the `solve_ivp` method from `scipy` was used. We start with an initial condition picked randomly from the ranges of initial conditions for state variables of each system mentioned in Appendix D. The number of initial conditions picked corresponds to the number of trajectories generated (Trajectories column in Table 2). The solver integrates differential equations to predict states of the system a certain number of time steps into the future (Timesteps column in Table 2). The dynamics of the system are discretized to predict the next step based on the current one. The time difference between the current and next step is denoted by Δt in Table 2.

Model	Δt	Timesteps	Trajectories
Lotka Volterra	0.1	300	500
Lorenz	0.01	300	1000
FHN	0.5	400	350
Lorenz95	0.01	300	666
Glycolytic	0.01	400	1000

Table 2. Details about data generation

D. Dynamical Systems

There are five dynamical systems studied in this paper. One of those is Lotka-Volterra (LV) equations, which are already discussed in section 2.2 along with its closed form, parameters, and ranges of initial conditions. Here, we repeat the description of the LV system and then describe the rest of the systems.

D.1. Lotka-Volterra (Wangersky, 1978)

$$\frac{dx}{dt} = \alpha x - \beta xy \quad (7)$$

$$\frac{dy}{dt} = \delta xy - \gamma y \quad (8)$$

Parameters: $\alpha = 1.1; \beta = 0.4; \gamma = 0.4; \delta = 0.1$

Initial Condition Ranges: $x \in [5, 20]; y \in [5, 10]$

D.2. Lorenz (Brunton et al., 2016)

$$\frac{dx}{dt} = \sigma(y - x) \quad (9)$$

$$\frac{dy}{dt} = x(\rho - z) - y \quad (10)$$

$$\frac{dz}{dt} = xy - \beta z \quad (11)$$

Parameters: $\sigma = 10; \rho = 28; \beta = \frac{8}{3}$

Initial Condition Ranges: $x \in [-20, 20]; y \in [-20, 20]; z \in [0, 50]$

D.3. FitzHugh-Nagumo (FHN) (Izhikevich & FitzHugh, 2006)

$$\frac{dv}{dt} = v - \frac{v^3}{3} - w + I \quad (12)$$

$$\frac{dw}{dt} = \epsilon(v + a - bw) \quad (13)$$

Parameters: $a = 0.7; b = 0.8; \epsilon = 0.08; I = 0.5$

IC Ranges: $v \in [-1.5, 1.5]; w \in [-1.5, 1.5]$

D.4. Lorenz95 (Lorenz, 1996)

$$\frac{dX_1}{dt} = (X_2 - X_5)X_4 - X_1 + F \quad (14)$$

$$\frac{dX_2}{dt} = (X_3 - X_1)X_5 - X_2 + F \quad (15)$$

$$\frac{dX_3}{dt} = (X_4 - X_2)X_1 - X_3 + F \quad (16)$$

$$\frac{dX_4}{dt} = (X_5 - X_3)X_2 - X_4 + F \quad (17)$$

$$\frac{dX_5}{dt} = (X_1 - X_4)X_3 - X_5 + F \quad (18)$$

Parameters: $F = 8$

Initial Condition Ranges: $X_i \in [-10.5, 10.5]$ where $i \in \{1, 2, 3, 4, 5\}$

D.5. Glycolytic Oscillator (Daniels & Nemenman, 2015)

$$\frac{dS_1}{dt} = J_0 - \frac{k_1 S_1 S_6}{1 + (S_6/K_1)^q} \quad (19)$$

$$\frac{dS_2}{dt} = 2 \frac{k_1 S_1 S_6}{1 + (S_6/K_1)^q} - k_2 S_2 (N - S_5) - k_6 S_2 S_5 \quad (20)$$

$$\frac{dS_3}{dt} = k_2 S_2 (N - S_5) - k_3 S_3 (A - S_6) \quad (21)$$

$$\frac{dS_4}{dt} = k_3 S_3 (A - S_6) - k_4 S_4 S_5 - \kappa (S_4 - S_7) \quad (22)$$

$$\frac{dS_5}{dt} = k_2 S_2 (N - S_5) - k_4 S_4 S_5 - k_6 S_2 S_5 \quad (23)$$

$$\frac{dS_6}{dt} = -2 \frac{k_1 S_1 S_6}{1 + (S_6/K_1)^q} + 2k_3 S_3 (A - S_6) - k_5 S_6 \quad (24)$$

$$\frac{dS_7}{dt} = \psi \kappa (S_4 - S_7) - k S_7 \quad (25)$$

Parameters: $J_0 = 2.5; k_1 = 100; k_2 = 6; k_3 = 16; k_4 = 100; k_5 = 1.28; k_6 = 12$

$k = 1.8; \kappa = 13; q = 4; K_1 = 0.52; \psi = 0.1; N = 1; A = 4$

Initial Condition Ranges: $S_1 \in [0.15, 1.60]; S_2 \in [0.19, 2.16]; S_3 \in [0.04, 0.20]; S_4 \in [0.10, 0.35];$
 $S_5 \in [0.08, 0.30]; S_6 \in [0.14, 2.67]; S_7 \in [0.05, 0.10]$

E. Uncertainty Propagation Illustrations

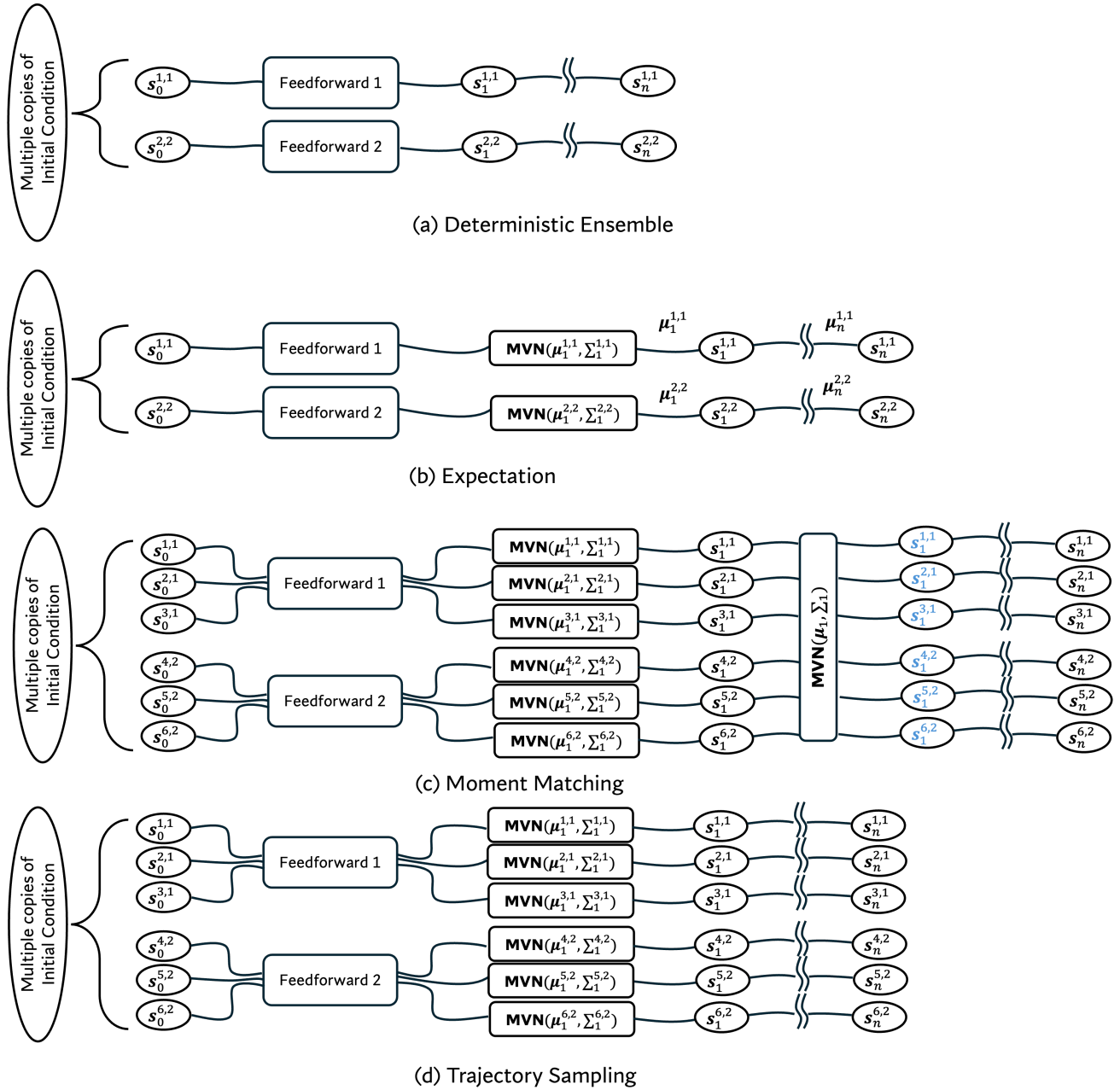


Figure 2. Uncertainty Propagation Illustrations

F. Details regarding Metrics

F.1. Calibration Error (CE)

A perfectly calibrated model has expected fractions of its predicted random variable perfectly matched with its observed fractions. That means that if we were to draw expected fractions on the x-axis and observed fractions on the y-axis, the resulting line should pass through the origin at an angle of $\frac{\pi}{4}$ (the dotted black line in Figure 6). This corresponds to a perfectly calibrated line. Any other curve (or line) deviating from this would count as miscalibration. The difference between a miscalibrated curve and a perfectly calibrated one is known as calibration error (CE). To calculate CE, we select $m = 9$ equally spaced PIs ranging from 10% to 90%. For each PI, we will count the number of times the observed variable falls between predicted PIs. For example, if we pick 90% PI, we expect the observed variable to fall between the predicted PI almost 90% of the time. For these 9 PIs, we would subtract expected and observed fractions, square, and then add up to report CE. Mathematically, this can be written as:

$$\text{CE} = \sum_{i=1}^m (p_i - \hat{p}_i)^2 \quad (26)$$

where p_i and \hat{p}_i denotes the expected and observed fractions, respectively. The expected fractions correspond to the following set of points $\{\frac{i}{10} \mid i = 1, \dots, 9\}$.

F.2. Prediction Interval Width (PI-Width)

A calibrated model should also be sharp. Sometimes, it is trivial to reduce the calibration error by simply predicting the expectation of a random variable, that is, $\mathbb{E}[Y]$. For example, if it rains 30 days out of 100 in a particular region, a weather forecaster always predicting a 30% chance of rain is calibrated. However, such a forecaster does not provide any actionable information and this information is not “sharp”. The forecaster should predict a probability close to 1 if it is very likely to rain and close to 0 if it is less likely to rain. Therefore, sharpness should be measured along with CE to assess the PI qualities. We propose to use prediction interval width (PI-width), which is commonly used in the conformal prediction literature (Angelopoulos et al., 2023), to assess the sharpness. Mathematically, it can be defined as:

$$\text{PI-Width} = \frac{1}{m} \frac{1}{N} \sum_{j=1}^m \sum_{i=1}^N |U_j^i - L_j^i| \quad (27)$$

where N denotes the total number of points in the validation dataset, and m denotes the 9 equally spaced prediction intervals. The results are averaged across all prediction intervals and data points. The letters U_j^i and L_j^i denote the upper and lower prediction intervals for i^{th} datapoint and j^{th} PI.

F.3. Mean Squared Error (MSE)

While CE and sharpness are sufficient to evaluate the performance of prediction intervals, the accuracy of a predictive model is equally important. We therefore propose using MSE as another performance metric. As ensembles have been shown to boost the predictive performance of a model, and Lakshminarayanan et al. (Lakshminarayanan et al., 2017) show their merit in quantifying predictive uncertainty, it is justifiable to look at the MSE of the ensemble’s predictions along with their calibration and sharpness. Our approach learns the residuals of a deterministic one-step predictive model via MHN’s pattern-retrieval mechanism, and we show that it can have a competitive performance compared to ensembles in terms of MSE, sharpness, and calibration, outperforming in most cases.

G. Attention Span

To get calibrated error density estimates from MHN, a concept we call *Attention Span* plays a pivotal role. The *Attention Span* of MHN is decided based on the sequence length it was trained on. As discussed in section 3, MHN needs data in sequences to train. The sequence length is defined as the number of keys/queries in a sequence. Recall that keys/queries in a sequence may not necessarily be in their temporal order, and they were mixed randomly to train MHN like a pattern retrieval algorithm. An example of sequence length 8 is shown in the association matrix in Fig. 1. The *Attention Span* decides how far apart in the feature space MHN looks to find keys with similar values, which eventually translates into

the uncertainty of the value (predicted variable). To illustrate that, we have generated data from a sine function with heteroscedastic Gaussian noise as follows

$$(x, y) \rightarrow \left(x, y + \mathcal{N} \left(0, 0.2 \left| \sin \left(\frac{3}{2}x + \frac{\pi}{8} \right) \right| \right) \right)$$

In total, 6000 points were generated by sampling x_i 's uniformly from the following domain $[-\frac{5\pi}{2}, -\pi] \cup [\pi, \frac{5\pi}{2}]$. A feedforward model with 2 hidden layers (100 neurons in each) was used as an encoder to learn features based on similarity using the attention mechanism. The resulting sine curve is shown in Fig. 3(a). Fig. 3(b) & (c) show the effect of changing the sequence length of training data. When the sequence length is small (that is, 3), the MHN pays attention to the keys very close to the query ($X = 3.28$), as shown in Fig. 3(b). As the sequence length slightly increases, that is, 8, the MHN pays attention to keys far apart in Euclidean distance but similar in their values, that is, $\sin(3.28)$, as shown in Fig. 3(c). In both cases, the query is the same, that is, 3.28, but their *Attention Spans* are different because they are trained on different sequence lengths. This sequence length intuitively relates to the calibration of the model and must be tuned to get the calibrated uncertainty, as observed in the training data. We introduce it as a hyperparameter that can be tuned based on the calibration error.

A scoring rule should be able to learn the uncertainty in the training data, but that training is expensive for MHN. A PyTorch pseudocode is shared in the Appendix B, showing how the network is trained using `torch`. The MSE was used as a loss function. As shown in the association matrix in Fig. 1, each query gets exposed to a certain number of keys and pays attention to a certain number of them except its ground truth to predict the error. The resulting categorical distribution has probabilities that get multiplied with values to predict the error which then goes through MSE loss. An alternative way to train this is to expose each query to a large number of keys, say a sequence length of 1000, and then take samples from it to estimate the mean and variance for NLL loss. We have observed that the MHN pays attention to a significant number of keys when exposed to bigger sequence lengths, which leads to a bigger *Attention Span*, hence a higher uncertainty or underconfident model. Although the PyTorch pseudocode shows the use of *dropout* during training to introduce sparsity to avoid big *Attention Span*, it does not work as well as explicitly changing the sequence length. By using a large sequence length, taking samples from the categorical distribution, and using NLL as a loss, MHN might be able to learn the calibrated uncertainty and avoid explicit changes to the sequence length. This is an interesting avenue for future work.

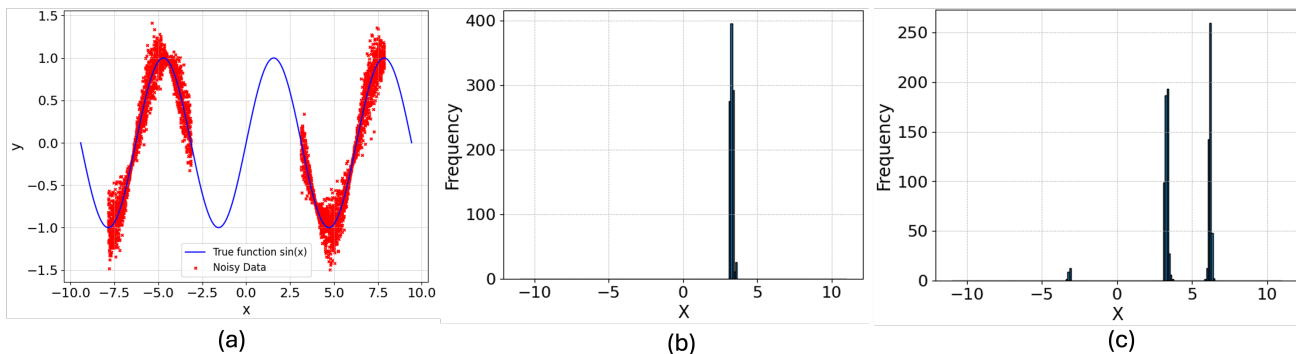


Figure 3. (a) Sine function with heteroscedastic noise (b) Attention Span at $X = 3.28$ with Sequence Length of 3 (c) Attention Span at $X = 3.28$ with Sequence Length of 8

H. MSE Table

Table 3 shows the MSEs of all systems at different levels of noise for HOPCAST and baseline methods.

Model		HOPCAST	Deterministic Ensemble	Probabilistic Ensemble		
				Expectation	Moment Matching	Trajectory Sampling
Metrics		MSE	MSE	MSE	MSE	MSE
Lotka Volterra	$\sigma = 0.05$	6.72 ± 0.32	24.34 ± 1.81	20.58 ± 1.25	28.9 ± 1.04	19.45 ± 0.36
	$\sigma = 0.1$	5.97 ± 0.04	23.8 ± 0.03	24.1 ± 0.15	23.9 ± 0.04	21.01 ± 0.27
	$\sigma = 0.3$	9.41 ± 0.23	25.4 ± 0.04	25.6 ± 0.09	25.4 ± 0.08	23.3 ± 0.05
Lorenz	$\sigma = 0.05$	1121 ± 7.97	1073.3 ± 23.85	1101.9 ± 28.3	1991.3 ± 4.03	1080.10 ± 5.59
	$\sigma = 0.1$	1254.2 ± 15	1420 ± 15.06	1413.1 ± 38.83	2579.7 ± 48.7	1314.60 ± 3.80
	$\sigma = 0.3$	1681 ± 46.36	1795 ± 17.36	1848.5 ± 15.8	2098.5 ± 18.08	1788.6 ± 10.9
FHN	$\sigma = 0.05$	0.049 ± 0.002	0.14 ± 0.006	0.68 ± 0.13	0.95 ± 0.45	0.66 ± 0.04
	$\sigma = 0.1$	0.17 ± 0.03	1.03 ± 0.24	1.39 ± 0.17	2.21 ± 0.13	0.83 ± 0.005
	$\sigma = 0.3$	0.60 ± 0.04	1.41 ± 0.07	1.53 ± 0.086	1.25 ± 0.003	1.12 ± 0.008
Lorenz 96	$\sigma = 0.05$	10.44 ± 0.08	9.77 ± 0.22	10.11 ± 0.21	14.11 ± 0.48	9.30 ± 0.031
	$\sigma = 0.1$	13.98 ± 0.11	13.77 ± 0.08	13.31 ± 0.20	17.38 ± 1.14	11.63 ± 0.11
	$\sigma = 0.3$	17.01 ± 0.66	17.33 ± 0.63	17.46 ± 0.11	16.37 ± 0.23	15.13 ± 0.075
Glycolytic Oscillator	$\sigma = 0.05$	0.03 ± 0.001	0.07 ± 0.003	0.10 ± 0.006	0.13 ± 0.019	0.09 ± 0.004
	$\sigma = 0.1$	0.06 ± 0.003	0.11 ± 0.002	0.12 ± 0.005	0.15 ± 0.005	0.10 ± 0.001
	$\sigma = 0.3$	0.12 ± 0.001	0.19 ± 0.007	0.18 ± 0.001	0.25 ± 0.002	0.17 ± 0.005

Table 3. Mean Squared Error (MSE) on different models with varying levels of noise across various models

I. Sequence lengths and Number of models

Table 4 shows the hyperparameters for HOPCAST and baseline methods. There are other hyperparameters, such as the number of layers in a feedforward model, etc.; we report the ones that we believe impact the CE, PI-Width, and MSE significantly.

Model	HOPCAST	Deterministic Ensemble	Probabilistic Ensemble			
			Expectation	Moment Matching	Trajectory Sampling	
Metrics	Sequence lengths	Models	Models	Models	Models	
Lotka Volterra	$\sigma = 0.05$	30,30,50,60	4	4	5	3
	$\sigma = 0.1$	70,30,70,40	6	5	5	3
	$\sigma = 0.3$	70,20,60,70	5	6	5	4
Lorenz	$\sigma = 0.05$	200 for all	7	8	7	3
	$\sigma = 0.1$	500,500,500,300,300,300	8	7	7	4
	$\sigma = 0.3$	25,25,25,500,500,500	7	8	7	3
FHN	$\sigma = 0.05$	35,55	4	5	5	3
	$\sigma = 0.1$	15,15	5	4	5	3
	$\sigma = 0.3$	15,15	5	5	4	3
Lorenz95	$\sigma = 0.05$	2200 for all	5	6	7	3
	$\sigma = 0.1$	2000 for all	6	6	5	4
	$\sigma = 0.3$	2000 for all	6	7	6	4
Glycolytic Oscillator	$\sigma = 0.05$	35,50,35,100,35,50,30	7	8	6	3
	$\sigma = 0.1$	50,50,35,35,800,35,100	8	6	7	3
	$\sigma = 0.3$	50 for all	6	7	8	3

Table 4. Sequence lengths for MHN and Number of models in an ensemble across various dynamical systems and noise levels

J. Performance Analysis

We have discussed the performance evaluation of different baselines against the MHN based on the proposed metrics, that is, CE and PI-Width, in section 5.3. Now, we will analyze their performance differences. First, let’s look at the error density estimates from MHN for x output of the Lorenz system. Fig. 4 shows the error densities of the underlying deterministic model’s output x at timesteps 106 and 297. As discussed earlier, MHN error densities can be added directly to the deterministic model’s prediction to get calibrated prediction intervals. Here, the underlying deterministic model’s predictions and ground truth are shown in dark and red colors, respectively, in Fig. 4. At timestep 106, the dark line is very close to the red line, and the error is very close to zero. The error density at that timestep is concentrated around zero with relatively lower uncertainty. On the other hand, the dark line is very far from the ground truth at timestep 297, resulting in a large error. The error density at that timestep is dispersed with a relatively higher uncertainty. This ability of MHN to pick similar patterns from its association memory at the inference time results in calibrated prediction intervals.

The average CEs of each model across all datasets are shown in the last row of Table 1. It can be seen that MHN and Trajectory Sampling are close in terms of average performance based on CE across all datasets. The performance of other baseline models differs significantly from MHN and Trajectory Sampling. These performance differences can be attributed to the densities approximated by the method at each timestep during autoregression. Let us discuss the densities of the predictive variable of interest, x at two different timesteps. The densities over the x output of the Lorenz system are shown in Fig. 5. The timesteps correspond to the trajectory shown in Fig. 4. For probabilistic models, a particle-based method was used to propagate uncertainty based on the predictive distribution. This was used only for Moment Matching and Trajectory Sampling because the propagation of expectation does not consider the uncertainty of the predictive distribution. So, the histograms are only plotted for these two methods. For the Lorenz system, we use an ensemble of 6 models with 20 particles for each model, resulting in 120 predictions at any timestep. The histogram is constructed based on these particles. The histograms for Moment Matching & Trajectory Sampling and density for MHN are plotted only at two timesteps. As shown in Fig. 5(a), the histogram frequency shows a Gaussian distribution for moment matching at timestep 270 and 297 of the trajectory shown in Fig. 4. Trajectory Sampling (Fig. 5(b)) and MHN (Fig. 5(c)) show approximate Gaussian

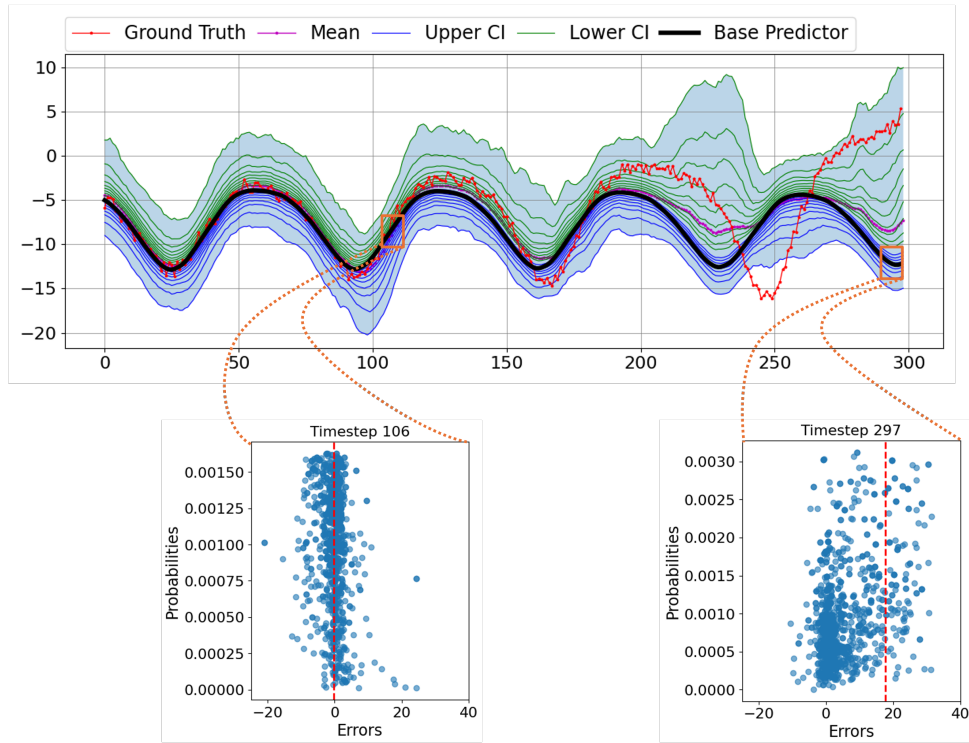


Figure 4. The predictive error density from MHN at particular timesteps

distributions with a single peak in density at timestep 270. On the other hand, both show a non-Gaussian distribution at timestep 270 in the face of higher uncertainty. This shows that the ability to capture non-Gaussian distributions at any timestep during autoregression is a key to getting calibrated multi-step predictions.

To evaluate the calibration performance of different models, we picked 9 prediction intervals from 10% to 90% with an increment of 10. The calibration curves of different models for the Glycolytic Oscillator at $\sigma = 0.3$ are shown in Fig. 6. The model's dynamics can be described with a system of 7 ODEs (Appendix D.5). The underlying deterministic model has 7 outputs, so calibration of all of them is quantified separately. The MHN shows a near-perfect calibration for all the outputs, whereas the trajectory sampling shows good calibration for a few outputs, three of which are miscalibrated. The rest of the methods do not show competitive performance. Although propagation of expectation and Trajectory Sampling performed the best almost equal number of times, Trajectory Sampling in general showed a lower CE in most cases (last row of Table 3).

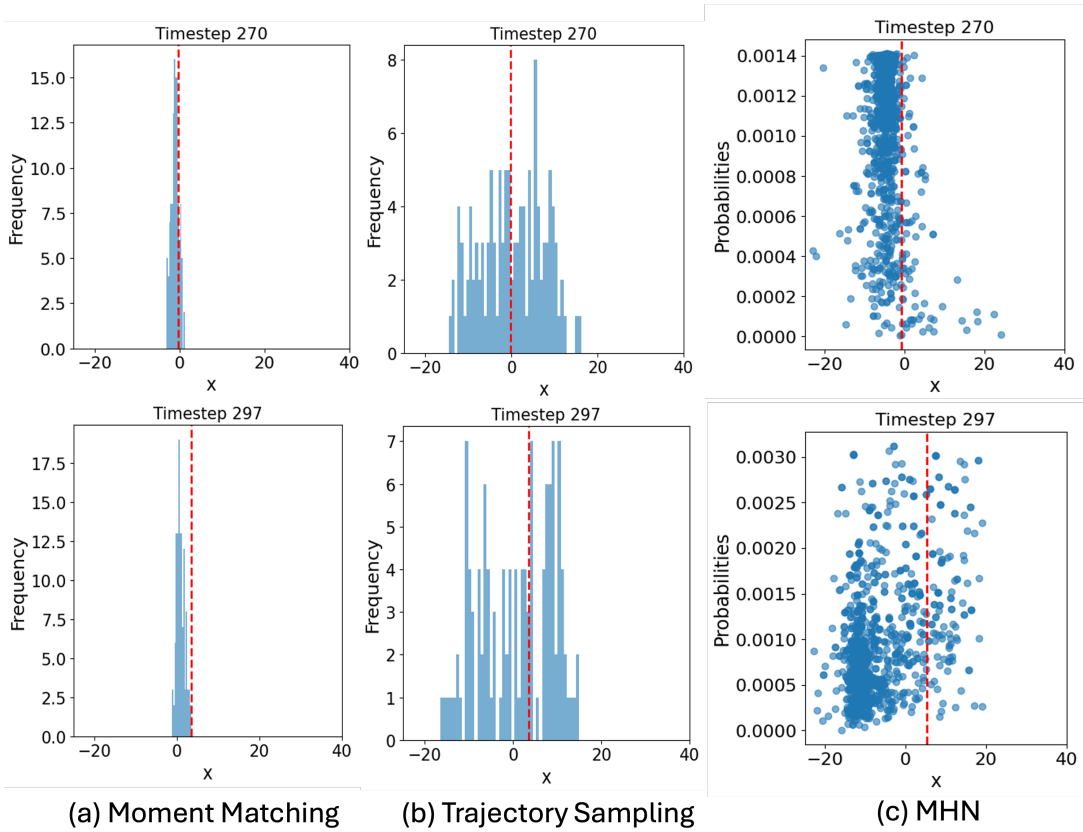


Figure 5. The densities of predictive variables x of Lorenz for different models

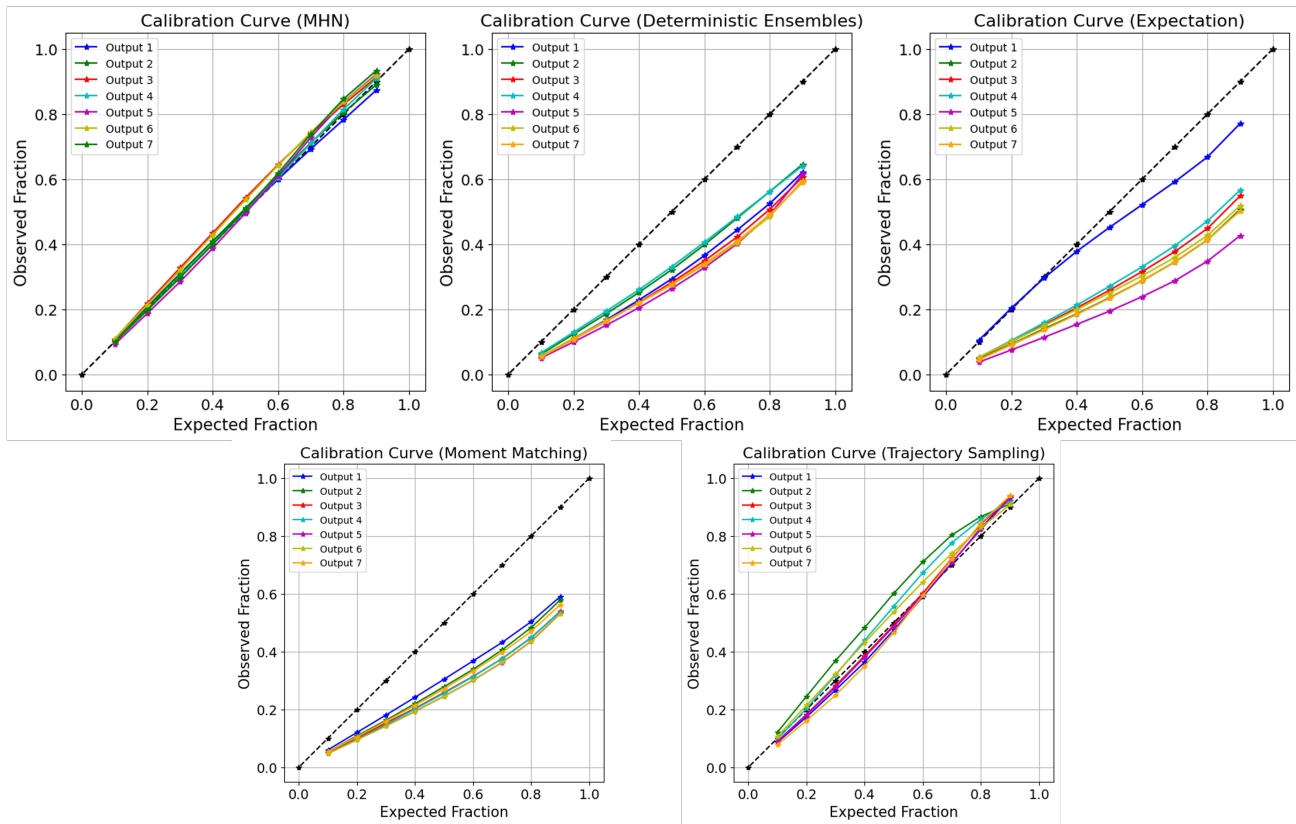


Figure 6. The calibration curves of different models for Glycolytic Oscillator at $\sigma = 0.3$. The dark dotted line corresponds to the perfect calibration.